Title

Dynamics of altruistic fluid transport in egg development

Authors

Imran Alsous J[1], Romeo N[2,^], Jackson J[1,3,^], Mason FM[4], Dunkel J[5,*], Martin AC[1,*].

Author affiliations

[1] Department of Biology, Massachusetts Institute of Technology, Cambridge, MA, 02139.

[2] Department of Physics, Massachusetts Institute of Technology, Cambridge, MA, 02139.

[3] Graduate Program in Biophysics, Harvard University, Cambridge, MA, 02138.

[4] Program in Cancer Biology, Vanderbilt University, Nashville, TN, 37232.

[5] Department of Mathematics, Massachusetts Institute of Technology, Cambridge, MA, 02139.

[^] Equal contribution

Corresponding authors

[*]acmartin@mit.edu, dunkel@mit.edu

Abstract

Interactions in which individuals benefit others at a cost to themselves are rife within the animal kingdom[1], from stalk cells in slime mold fruiting bodies[2] to social insect colonies where sterile workers live for the queen[3]. The development of an egg cell occurs within similarly self-sacrificing communes. Across species, oocytes develop within cysts alongside nurse-like germ cells; a key juncture in oogenesis occurs when these sister cells transport their cytoplasm to the oocyte prior to fertilization[4,5]. As a result, the oocyte grows as its sister cells regress and die[6]. Long observed in insects, recent work shows that development of the mammalian egg cell occurs through similar intercellular transport processes[7,8]. Although critical for fertility and embryonic life, the biological and physical mechanisms underlying such altruistic fluid transport remain poorly understood, owing to a lack of time-resolved quantitative data. Here, we combined e*x vivo* live imaging of germline cysts with mathematical modeling to investigate the dynamics and mechanisms that enable directional and complete cytoplasmic transport in *Drosophila melanogaster* egg chambers. We discovered that during 'nurse cell dumping', most cytoplasm is transported into the oocyte independently of changes in myosin-II contractility, with dynamics predicted by Young-Laplace's law, suggesting pressure-driven transport induced by baseline cell surface tension. A minimal flow network model inspired by the famous two-balloon experiment correctly predicts transport directionality and time scale. Long thought to trigger transport through 'squeezing'[9,10], increased actomyosin contractility is required only once cell volume is reduced by ~75%, in the form of cell peristaltic contractile waves that permit continued flow. Our work thus demonstrates how biological and physical mechanisms cooperate to enable proper cell and tissue level behaviours during a conserved act of cytoplasmic transport in early development.

Main text

The *Drosophila* oocyte develops within an egg chamber, a multicellular structure that comprises a germline cyst of 16 cells that are interconnected through intercellular bridges called ring canals and covered by an epithelium (Fig. 1a)[11-13]. After the oocyte grows to ~50% of the egg chamber's volume, all 15 sister germ cells, called nurse cells, transport the entirety of their contents directionally into the oocyte

in a process called 'nurse cell (NC) dumping'; with a diameter of ~10 μm, ring canals are large enough to permit passage of most cytoplasmic contents (Fig. 1b; Extended Data Fig. 1a; Supplementary Video 1)[14]. It is thought that NC dumping is driven by global cortical contractile forces generated through interactions of non-muscle myosin II (myosin) with actin filaments (henceforth actomyosin), i.e. through an increase in pressure, cytoplasm is 'squeezed' out of the NCs and into the oocyte[9,10]. While mutants in the myosin regulatory light chain (RLC), encoded for by the *spaghetti squash* (*sqh*) gene, do not complete NC dumping[15,16], the mechanisms underlying the complete and directional pattern of intercellular transport are unknown, and actomyosin's role in promoting this process is unclear.

Using *ex vivo* live imaging of egg chambers with simultaneously labeled membranes (*Ecad::GFP*), myosin (*sqh::mCH*), and cytoplasm (*Clip170::GFP*), we determined the dynamics of NC dumping and corresponding patterns of actomyosin activity. First, through size measurements of the oocyte and the 15 NCs (Extended Data Fig. 1a-d), we found that NC dumping unfolds over the course of ~100 minutes, a period ~3-fold longer than previously reported indirect estimates[17,18]. We also found that NCs empty ~75% of their volume into the oocyte through spatially uniform shrinkage of the cells, in the absence of nonuniform cell shape changes and membrane blebbing that imply local contractile force generation. In contrast, transport of the remaining cytoplasm is accompanied by dynamic and persistent NC shape deformations (Fig. 1c, d; Extended Data Fig. 2; Supplementary Video 2).

Similarly, we found that NC dumping onset occurs without changes to myosin level and localization pattern as compared to the previous developmental stage. NCs' cortical myosin reorganizes from a uniform to a nonuniform dynamic cortical pattern only ~40 minutes into NC dumping, coincident with the onset of dynamic cell shape deformations (Fig. 1e; Supplementary Video 3; Extended Data Fig. 3a, b); no such changes were observed in control membrane makers (Extended Data Fig. 3c). NC dumping therefore unfolds in two distinct phases, only the latter of which coincides with changes to actomyosin-mediated cell contractions.

We next explored mechanisms whereby directional intercellular fluid flow can occur in the absence of peristalsis-like cell deformations mediated through dynamic actomyosin contractility. To that end, we first determined the spatiotemporal pattern of intercellular cytoplasmic transport and found that NC dumping unfolds in a hierarchical manner that correlates with the NCs' size and arrangement. At NC

dumping onset, the oocyte is the largest cell in the egg chamber; however, the NCs, which are arranged in four layers (L1-L4; Fig. 2a), also exhibit a descending cell size order according to their distance from the oocyte[19-21]. Our data show that NCs directly connected to the oocyte, i.e., L1 cells, are first to transport their contents into the oocyte, followed in order by smaller NCs in layers L2-L4 (Fig. 2b, c).

Driven by our experimental observations, in which smaller cells empty their contents into larger ones prior to changes in myosin localization and cell shape deformations, we developed a pressure-driven networked-flow model that was inspired by the two-balloon problem: if two identical balloons inflated to different volumes are allowed to exchange air, the smaller balloon will empty its contents into the larger balloon that grows at its expense (Fig. 2d). This seemingly counter-intuitive phenomenon can be explained by the Young-Laplace law, which states an inverse relationship between pressure p and radius R for a sufficiently large balloon; taking into account the hyperelastic behaviour of rubber, the pressure inside the inflated balloon is then given by:

$$p = \frac{2\gamma}{R}\left(1 - \left(\frac{R_0}{R}\right)^6\right) \quad (1)$$

where R_o is the radius of the uninflated balloon and γ its surface tension (Fig. 2d)[22,23]. To apply this description to our biological system, we assumed that the cells are roughly spherical[24] and that membranes are incompressible and adequately described by a passive neo-Hookean material under static loading[25] (*Methods*).

The two-balloon problem is then readily extended to the germline cyst that can be represented as a 16-cell network (Fig. 2e), where the pressure-driven flux J_{ij} from cell j to i through a cylindrical ring canal of radius r_{ij} and length L is given by:

$$J_{ij} = G_{ij}(p_j - p_i) \quad (2)$$

with a hydraulic conductance $G_{ij} \propto r_{ij}^4/L$ for Poiseuille-type flow *(26)*. Tension in this description arises from a combination o in-plane tension of the plasma membrane and tension present in the actomyosin cortex. Using experimentally determined cell sizes at onset of NC dumping as initial conditions[20], we numerically solved the transport equations for the evolution of cell volumes V_i in the 16-cell tree:

$$\frac{dV_i}{dt} = \sum_{\langle i,j \rangle} J_{ij} = \sum_{\langle i,j \rangle} G_{ij}(p_j - p_i) \quad (3)$$

where the sum runs over connected cell neighbors i and j.

Despite its minimal character, the flow-network model robustly captures qualitatively essential features of the experimentally observed transport dynamics (Extended Data Fig. 4a, b; *Methods*). Specifically, the model correctly predicts both the hierarchical pattern of intercellular transport and timescale of NC dumping (Fig. 2f). By also accounting for natural cell-to-cell variability in effective cell surface tension[27], the proposed model successfully captures experimentally observed complex transport patterns along the 16-cell tree. For example, our data show the L4 NC transiently increasing in size during NC dumping, which can occur if the L3 cell to which it is connected shrinks sufficiently such that it becomes smaller than the L4 cell. Such transient back flow away from the oocyte is a feature of NC dumping that has been documented before[28] and is predicted by our model (Extended Data Fig. 4c, Supplementary Video 4).

A novel insight into NC dumping provided by the model is the high sensitivity of intercellular transport to changes in ring canal size through quartic scaling of the hydraulic conductance. By reconstructing ring canal growth dynamics, we show that ring canals reach ~10-fold their initial size throughout oogenesis, consistent with previous studies[12], but also that they do so rapidly prior to the onset of NC dumping (Extended Data Fig. 5a). NC dumping onset, thought to be a sudden event, is thus possibly triggered by an increase in effective ring canal size, which sharply accelerates ongoing cytoplasmic transport from nurse cells into the oocyte (Extended Data Fig. 5b). Notably, prior to NC dumping, microtubules that emanate from the microtubule organizing center (MTOC) in the oocyte and extend into the NCs through ring canals[29] are disassembled and reassembled along the oocyte cortex[30], thus further increasing the effective radius of the ring canals prior to the onset of rapid transport (Extended Data Fig. 5c).

Our model and the Young-Laplace law predict that lowering of the effective NC surface tension will slow down the rate of intercellular transport but will not affect transport directionality or hierarchical order. To further test that NC dumping onset and transport directionality are not caused by changes in actomyosin contractility, we quantified the spatiotemporal pattern of NC dumping in *sqh*^{1} mutant germline clones, where endogenous Sqh mRNA and protein levels are reduced by ~90%[31,32]. We found that while Sqh depleted germline cysts exhibit a ‘dumpless’ phenotype, i.e., do not complete NC dumping (Fig.

2g)[15], the hierarchical transport pattern observed during Phase I in WT is largely maintained (Fig. 2h, i; Supplementary Video 5). This observation is consistent with myosin contributing to the baseline level of cortical tension, but not the direction or order of intercellular cytoplasmic transport. Indeed, we find that NC dumping in *sqh*^{1} mutants, while maintaining the order of transport observed in WT, proceeds more slowly, suggesting that it is driven by surface tension-generated pressure differences (Fig. 2i, inset).

The fact that *sqh*^{1} mutants are dumpless suggests that physical mechanisms alone (i.e., passive surface tension and the relationship between pressure and radius) are insufficient for complete cytoplasmic transport, and that actomyosin dynamics and regulation are critical. Through live imaging of egg chambers with labeled myosin (*sqh::mCH*) and actin (*F-tractin::TdTomato* and *Utr::GFP*), we found that during Phase II of NC dumping, actomyosin contractility is highly dynamic, exhibiting a diversity of spatiotemporally organized cortical waves, such as colliding myosin wave fronts, rotating cortical bands, and myosin rings travelling between the cell's poles, which dynamically deform NC shape (Fig. 3a-e; Supplementary Video 6). We also found that actomyosin waves in the NCs travel at ~0.3 μm/s, a speed comparable to that of Rho-actin contraction waves observed in frog and starfish oocytes and embryos[33]. Notably, the intercellular pattern of actomyosin wave onset mirrors that of cytoplasmic transport, starting in NCs closer to the oocyte, i.e., those that shrink first, before appearing in further cells (Fig. 3f).

Dynamic actomyosin behaviours like those observed here are regulated through RhoA activation and inhibition and feedback through advection[33-35]. RhoA is a small GTPase activated by guanine nucleotide exchange factors (GEFs) and inhibited by GTPase-activating proteins (GAPs)[36,37]. Binding to downstream effectors, such as the Rho-associated and coiled-coil kinase (ROCK; Rok in *Drosophila*), results in increased contractility through myosin RLC phosphorylation (Fig. 3g)[38-40]. Our data show that similar to myosin, Rok, Utrophin, and F-Tractin also exhibit wave-like behaviour (Extended Data Fig. 6a-c; Supplementary Video 7), suggesting that dynamic RhoA regulation, rather than constitutive caspase cleavage-mediated activation of Rok[41], underlies myosin's observed dynamics. Furthermore, through a genetic screen, we identified RhoGAP15B, the *Drosophila* homolog of ARAP1/3, as a critical regulator of wave dynamics[34]; the RhoGAP domain of the human RhoGAP15B homolog exhibits highest specificity towards RhoA[42], consistent with RhoGAP15B regulating actomyosin contractility. We found that while RhoGAP15B depletion in the germline cyst led to a 'dumpless' phenotype (Fig. 3h), onset of NC dumping

and the hierarchical pattern of transport during Phase I were unaffected, although there was greater variability in knockdown egg chambers (Fig. 3i). Instead, RhoGAP15B depletion led to disruption of myosin wave dynamics and concomitant cell-scale shape deformations otherwise observed during Phase II in WT; cells displayed erratic myosin activity associated with smaller and more transient cell protrusions (Fig. 3j, k; Supplementary Video 8). We confirmed that incomplete NC dumping in RhoGAP15B knockdowns is not attributable to obstructed or diminished ring canal sizes, or disrupted actin cables (Extended Data Fig. 7)[43]. Taken together, these data suggest that incomplete cytoplasmic transport is due to disrupted wave dynamics in Phase II of NC dumping.

A clue to actomyosin's role in completing NC dumping came from directly visualizing inter- and intracellular cytoplasmic flow using reflection-mode microscopy. Following actomyosin wave onset and concomitant NC shape deformations (Fig. 4a), cytoplasm was observed squeezing through spaces between NC nuclei and membranes and completing multiple revolutions around the nucleus as intercellular anterior-to-posterior transport continued (Fig. 4b, c; Supplementary Video 9). In contrast, intracellular flow in RhoGAP15B knockdowns appeared erratic and lacked the persistent radial motions around NC nuclei necessary for bringing cytoplasm in contact with a ring canal (Fig. 4d, e). As a result, RhoGAP15B knockdowns exhibited interrupted anterior-to-posterior intercellular flow, more frequent transport of cytoplasm away from the oocyte (Fig. 4f, g; Supplementary Video 10), a greater degree of layer 4 expansion (Fig. 3i), and incomplete NC dumping. Given that actomyosin waves first appear in a nurse cell once it has emptied most of its cytoplasmic contents (Fig. 3f, Extended Data Fig. 2e), we hypothesize that wave-mediated NC deformations prevent blockage and enable complete NC dumping by creating spaces between shrunken NC plasma membranes and nuclei, thus creating a path that connects anterior to posterior ring canals for continued directional transport (Fig. 4h).

To conclude, the above analysis demonstrates how physical and biological mechanisms jointly facilitate oocyte development. Our experiments and theory show that tension-driven flows provide robust and highly tunable fluid-mechanical control over directional intercellular cytoplasmic flow and that subsequent wave-like actomyosin contractions are essential to complete transport. Our data and proposed model contrast with current hypotheses for NC dumping in which cytoplasm is driven out of the NCs through a global increase in pressure mediated through cytoskeletal force generation[28]; in such a

model, NC pressure in cells closest to the oocyte is decreased through loss of cytoplasm into the oocyte, allowing further transport from more distal cells. Such a model however does not mechanistically explain the directionality and hierarchical flow observed during NC dumping and postulates that actomyosin contractility increase at the onset of NC dumping, which our data show does not occur until the NCs have emptied most of their cytoplasmic contents into the oocyte.

Our results also reveal a previously unknown function for actomyosin dynamics during oogenesis and expands the repertoire of roles played by surface cortical waves and excitable myosin dynamics in development[35,44-46]. The observed diversity of actomyosin waves reported here is similarly novel, and opens up avenues for investigating the dynamics of wave propagation on complex and deformable surfaces – an area of research long active within acoustics and optics for example, but only recently explored in biological contexts[47]. Sisterly sacrifice among germ cells has been shown to occur in insects and in mammals[4,5,7]; we therefore expect the above results to translate to other organisms. Lastly, from a broader conceptual perspective, our study highlights the complementary important roles of physical and biological processes in driving proper cell and tissue level behaviours during early development.

References

1. Darlington, P.J. Altruism: Its characteristics and evolution. *Proc. Natl. Acad. Sci. U.S.A.* **75**, 385–389 (1978).
2. Strassmann, J.E., Zhu, Y. & Queller, D.C. Altruism and social cheating in the social amoeba *Dictyostelium discoideum. Nature* **408**, 965–967 (2000).
3. Hamilton, W.D. Altruism and related phenomena, mainly in social insects. *Annu. Rev. Ecol. Syst*. **3**, 193–232 (1972).
4. Telfer, W. H. Development and physiology of the oocyte-nurse cell syncytium. *Adv. Insect Physiol.* **11**, 223–319 (1975).
5. Pepling, M.E., de Cuevas, M. & Spradling, A.C. Germline cysts: a conserved phase of germ cell development? *Trends Cell Biol.* **9**, 257–262 (1999).
6. Jenkins, V.K., Timmons, A.K. & McCall, K. Trends in Diversity of cell death pathways: insight from the fly ovary. *Trends Cell Biol.* **23**, 567–574 (2013).

7. Lei, L. & Spradling, A.C. Mouse oocytes differentiate through organelle enrichment from sister cyst germ cells. *Science* **352**, 95–99 (2016).
8. Sun, Y.C., Cheng, S.F., Sun, R., Zhao, Y. & Shen, W. Reconstitution of gametogenesis *in vitro*: meiosis is the biggest obstacle. *J. Genet. Genomics* **41**, 87–95 (2014).
9. Guild, G. M., Connelly, P. S., Shaw, M. K. & Tilney, L.G. Actin filament cables in *Drosophila* nurse cells are composed of modules that slide passively past one another during dumping. *J. Cell Biol.* **138**, 783–797 (1997).
10. Gutzeit, H. O. & Koppa, R. (1982). Time-lapse film analysis of cytoplasmic streaming during late oogenesis of *Drosophila. J. Embryol. Exp. Morphol.* **67**, 101–111 (1982).
11. Bastock, R. & St Johnston, D. *Drosophila* oogenesis. *Curr. Biol.* **18**, 1082–1087 (2008).
12. King, R.C. Ed., *Ovarian Development in Drosophila melanogaster*. (Academic Press, New York, NY, 1970).
13. Spradling, A.C. “Developmental genetics of oogenesis” in *The Development of Drosophila melanogaster*, M. Bate, A. Martinez Arias, Eds. (Cold Spring Harbor Press, Plainview, NY, 1993) vol. 1, pp. 1–70.
14. Theurkauf, W. E. & Hazelrigg, T. I. *In vivo* analyses of cytoplasmic transport and cytoskeletal organization during Drosophila oogenesis: characterization of a multi-step anterior localization pathway. *Development* **125**, 3655-3666 (1998).
15. Wheatley, S., Kulkarni, S. & Karess, R. *Drosophila* nonmuscle myosin II is required for rapid cytoplasmic transport during oogenesis and for axial nuclear migration in early embryos. *Development* **121**, 1937–1946 (1995).
16. Edwards, K.A. & Kiehart, D.P. *Drosophila* nonmuscle myosin II has multiple essential roles in imaginal disc and egg chamber morphogenesis. *Development* **122**, 1499–1511 (1996).
17. David, J. & Merle, J. A reevaluation of the duration of egg chamber stages in oogenesis of *Drosophila melanogaster*. *Drosophila Inf. Serv.* **43**, 122 (1968).
18. Lin, H. & Spradling, A.C. Germline stem cell division and egg chamber development in transplanted *Drosophila* germaria. *Dev. Biol.* **159**, 140–152 (1993).

19. Imran Alsous, J., Villoutreix, P., Stoop, N., Shvartsman, S.Y. & Dunkel, J. Entropic effects in cell lineage tree packings. *Nat. Phys.* **14**, 1016–1021 (2018).
20. Imran Alsous, J., Villoutreix, P., Berezhkovskii, A.M. & Shvartsman, S.Y. Collective growth in a small cell network. *Curr. Biol.* **27**, 2670–2676 (2017).
21. Brown, E.H. & King, R.C. Studies on the events resulting in the formation of an egg chamber in *Drosophila melanogaster*. *Growth* **28**, 41–81 (1964).
22. Merrit, D.R. & Weinhaus, F. The pressure curve for a rubber balloon. *Am. J. Phys.* **46**, 976–977 (1978).
23. Verron, E., Khayat, R. E., Derdouri, A. & Peseux, B. Dynamic inflation of hyperelastic spherical membranes. *J. Rheol.* **43**, 1083–1097 (1999).
24. Tu, K.-N. & Gusak, A. M. “Appendix A: Laplace Pressure in Nonspherical Nanoparticle” in *Kinetics in Nanoscale Materials* (Wiley, New Jersey, ed. 2, 2014), pp. 280–281.
25. Hu, J., Chen, S., Hu, W., Lü, S. & Long, M. Mechanical point loading induces cortex stiffening and actin reorganization. *Biophys. J.* **117**, 1405–1418 (2019).
26. Acherson, D.J. *Elementary Fluid Dynamics* (Clarendon Press, Oxford, 1990).
27. Lamiré, L.-A. *et al*. Gradient in cytoplasmic pressure in the germline cells controls overlying epithelial cell morphogenesis. Preprint at https://www.biorxiv.org/content/10.1101/440438v2 (2020).
28. Gutzeit, H. O. The role of microfilaments in cytoplasmic streaming in *Drosophila* follicles. *J. Cell Sci.* **80**, 159–169 (1986).
29. Grieder, N.C., de Cuevas, M. & Spradling, A.C. The fusome organizes the microtubule network during oocyte differentiation in *Drosophila. Development* **127**, 4253–4264 (2000).
30. Theurkauf, W.E., Smiley, S., Wong, M.L. & Alberts, B.M. Reorganization of the cytoskeleton during *Drosophila* oogenesis: implications for axis specification and intercellular transport. *Development* **115**, 923–936 (1992).
31. Karess, R.E. *et al*. The regulatory light chain of nonmuscle myosin is encoded by spaghetti-squash, a gene required for cytokinesis in *Drosophila*. *Cell* **65**, 1177–1189 (1991).
32. Vasquez, C.G., Tworoger, M. & Martin, A.C. Dynamic myosin phosphorylation regulates contractile pulses and tissue integrity during epithelial morphogenesis. *J. Cell Biol.* **206**, 435–450 (2014).

33. Bement, W.M. *et al*. Activator-inhibitor coupling between Rho signaling and actin assembly makes the cell cortex an excitable medium. *Nat. Cell Biol.* **17**, 1471–1483 (2015).
34. Mason, F.M., Xie, S., Vasquez, C.G., Tworoger, M. & Martin, A.C. RhoA GTPase inhibition organizes contraction during epithelial morphogenesis. *J. Cell Biol.* **214**, 603–617 (2016).
35. Munjal, A., Philippe, J.-M., Munro, E. & Lecuit T. A self-organized biomechanical network drives shape changes during tissue morphogenesis. *Nature* **524**, 351-355 (2015).
36. Bos, J.L., Rehmann, H. & Wittinghofer, A. GEFs and GAPs: critical elements in the control of small G proteins. *Cell* **129**, 865–877 (2007).
37. Cook, D.R., Rossman, K.L. & Der, C.J. Rho guanine nucleotide exchange factors: regulators of Rho GTPase activity in development and disease. *Oncogene* **33**, 4021–4035 (2014).
38. Kimura, K. *et al.* Regulation of myosin phosphatase by Rho and Rho-associated kinase (Rho-kinase). *Science* **273**, 245–248 (1996).
39. Winter, C.G. et al. *Drosophila* Rho-associated kinase (Drok) links Frizzled-mediated planar cell polarity signaling to the actin cytoskeleton. *Cell* **105**, 81–91 (2001).
40. Amano, M. *et al*. Phosphorylation and activation of myosin by Rho-associated kinase (Rho-kinase). *J. Biol. Chem.* **271**, 20246–20249 (1996).
41. Sebbagh, M. *et al.* Caspase-3-mediated cleavage of ROCK I induces MLC phosphorylation and apoptotic membrane blebbing. *Nat. Cell Biol*. **3**, 346–352 (2001).
42. Miura, K. *et al.* ARAP1: a point of convergence for Arf and Rho signaling. *Mol. Cell*. **9**, 109–19 (2002).
43. Huelsmann, S., Ylänne, J. & Brown, N.H. Filopodia-like actin cables position nuclei in association with perinuclear actin in *Drosophila* nurse cells. *Dev. Cell* **26**, 604–615 (2013).
44. Michaux, J.B., Robin, F.B., McFadden, W.M. & Munro, E.M. Excitable RhoA dynamics drive pulsed contractions in the early *C. elegans* embryo. *J. Cell. Biol.* **217**, 4230–4252 (2018).
45. Bischof, J. *et al.* A cdk1 gradient guides surface contraction waves in oocytes. *Nat. Comm.* **8**, 849 (2017).
46. Martin A. C., Kaschube M. & Wieschaus, E. F. Pulsed contractions of an actin-myosin network drive apical constriction. *Nature* **457**, 495–9 (2009).

47. Miller, P. W., Stoop, N. & Dunkel, J. Geometry of wave propagation on active deformable surfaces. *Phys. Rev. Lett.* **120**, 268001 (2018).

Supplementary Information is available for this paper.

Correspondences and requests for materials can be addressed to acmartin@mit.edu, dunkel@mit.edu, and jasmini@mit.edu.

Acknowledgements We thank Stefan Muenster (Max Planck Institute, Dresden) and Wendy Salmon (Whitehead Institute, Keck Microscopy Facility) for advice regarding use of reflection-mode microscopy. We thank Clint Ko and Jaclyn Camuglia for assistance with experiments, and Alexander Mietke for discussions on wave-driven cytoplasmic flows. We are grateful to Stanislav Y. Shvartsman and Miriam Osterfield for comments on the manuscript. This work was supported by the Molecular Biophysics Training Grant (National Institute of General Medical Sciences, T32 GM008313) (J.J.), a Complex Systems Scholar Award from the James S. McDonnell Foundation (J.D.), and National Institute of General Medical Sciences grant R01-GM125646 (A.C.M).

Author contributions J.I.A. conceptualized the project. J.I.A. and A.C.M. designed the experimental pipeline. J.I.A. and J.J. performed the experiments with input from N.R., J.D., and supervision by A.C.M. J.I.A and J.J. analysed the experimental data. J.J. developed the computational framework for quantitative analysis of NC dumping dynamics. J.D. and N.R. developed the computational model. N.R. performed simulations, for which J.I.A. and J.J. provided data. F.M. performed the genetic screen that identified RhoGAP15B as an essential GAP for NC dumping. J.I.A. wrote the first draft of the paper. All authors discussed and revised the manuscript.

Competing interests: The authors declare no competing interests.

Data and materials availability: The code used for numerical simulations is available on a public repository at https://github.com/NicoRomeo/balloon-dynamics. All experimental data are available in the main text or the supplementary materials.

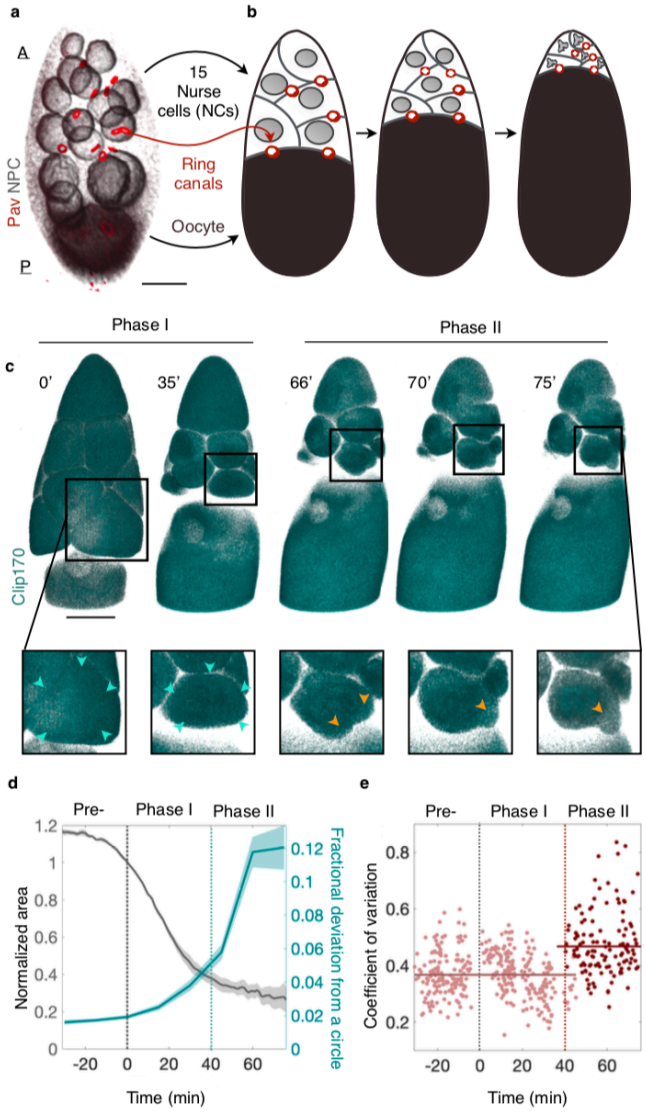

Figure 1 | Nurse cell (NC) dumping unfolds in two distinct phases. **a**, 3D-rendered confocal image of an egg chamber comprising 15 anterior (A) NCs (*Nuclear pore complex, NPC*; gray) and one posterior (P) oocyte (black) connected through ring canals (*Pavarotti, Pav*; red). **b**, Schematic illustration of NC dumping: NCs shrink as their cytoplasm flows into the oocyte through ring canals over ~100 minutes (Extended Data Fig. 1a). **c**, 3D-rendered time-lapse confocal images of an egg chamber expressing *Clip170::GFP*. Blowups show a cell first shrinking uniformly (cyan arrowheads; Phase I) before undergoing spatially nonuniform shape deformations and bleb-like protrusions (yellow arrowheads; Phase II) that imply local force generation. Scale bar in **a** and **c** = 40 μm. **d**, Quantification of changes in cell size (gray) and changes cell shape (i.e. fractional deviation from a circle; Extended Data Fig. 2c) prior to NC

dumping (Pre-), and during Phases I and II. Onset of non-uniform deformations (dashed cyan line) occurs ~40 minutes into NC dumping for the samples analysed ($N = 4$). **e**, Coefficient of variation of cortical Sqh intensity during 'NC dumping', showing a transition (dashed red line) from uniform ($N = 412$; Phase I) to non-uniform ($N = 122$; Phase II) distribution at ~40 minutes into NC dumping, concomitant with onset of dynamic cell shape deformations.

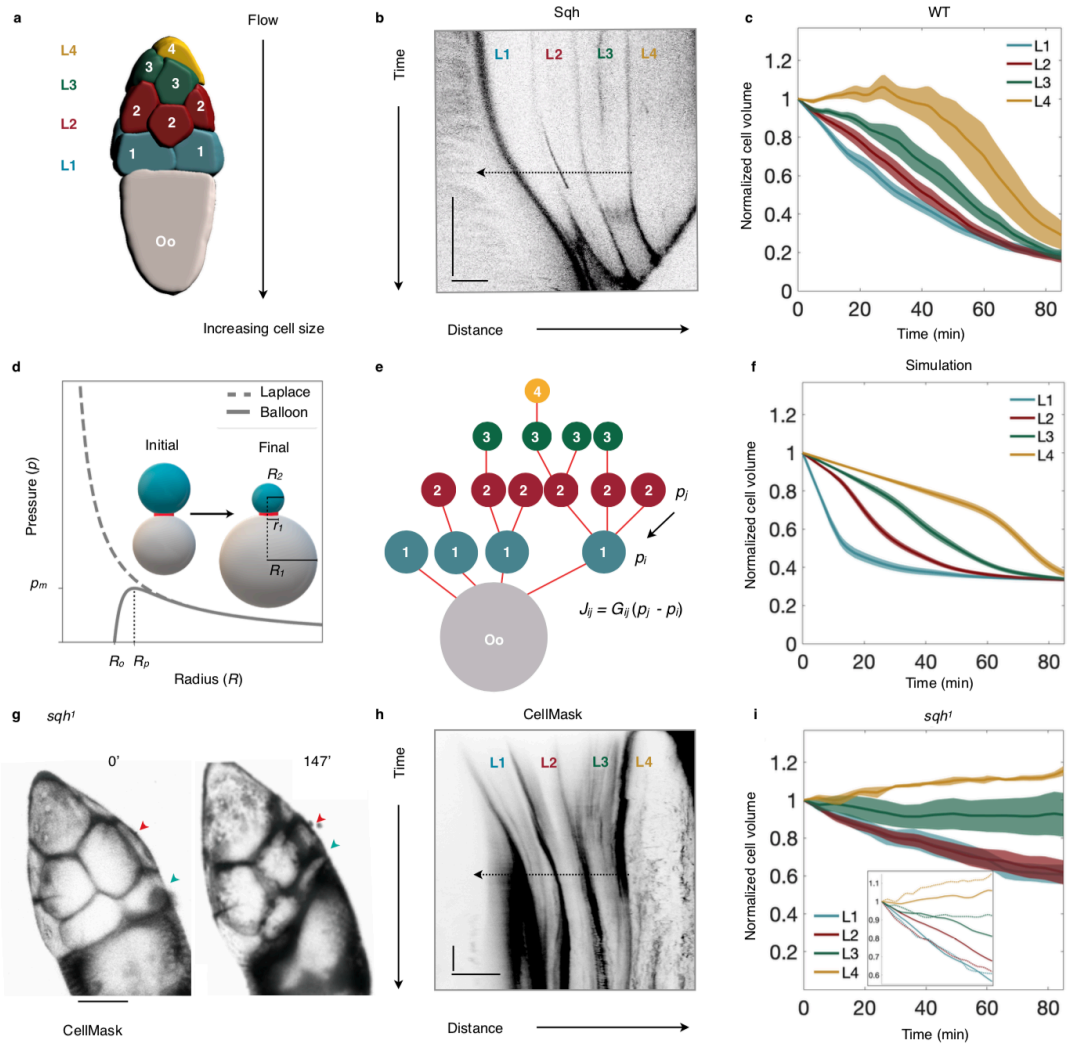

Figure 2 | A pressure-driven networked-flow model explains dynamics of Phase I of NC dumping. **a**, 3D-reconstruction of a germline cyst showing the NCs' arrangement into four layers relative to the oocyte (Oo). During NC dumping, cytoplasm flows in direction of increasing cell size. **b**, Kymograph of Sqh intensity in WT, illustrating hierarchical onset of NC dumping across the layers; dashed arrow indicates direction of flow. Scale bars = 30 min, 50 μm; black indicates highest intensity. **c**, Plot of normalized NC volumes (V/V_o) during NC dumping for each layer from live imaging; t = 0 is onset of NC dumping; solid line indicates average; envelopes show standard error (N = 15, 12, 9, 5 cells for layers 1, 2, 3, and 4, respectively). **d**, Plots of Young-Laplace's law and the corrected pressure law for elastic balloons. Pressure is at its maximum, p_{max}, at radius R_p; R_o is the uninflated balloon radius; r_{12} is the radius of the pipe connecting balloons 1 and 2. Schematic illustrates the two-balloon problem, where the

smaller balloon (cyan) empties into the larger balloon (gray). **e**, Network representation of the germline cyst in **a** showing cells' relative sizes; cells are shown as nodes and ring canals as edges. **f**, Plot of normalized NC volumes from simulations using the best fit parameter set (solid line); envelopes show standard error constructed from the ten nearest sets in parameter space (N = 11). Time is scaled by the physical constants of the model. **g**, *sqh*^{1} germline mutant showing NCs in the first (blue arrowhead) and second (red arrowhead) layers emptying into the oocyte. **h**, Kymograph of CellMask intensity in *sqh*^{1} mutants, showing cytoplasmic transport from the first two layers. Scale bars = 30 min; 70 μm. **i**, Plot as in **c** of normalized NC volumes over time in *sqh*^{1} germline clones; (N = 14, 17, 7, 6 cells for layers 1, 2, 3, and 4, respectively); inset shows WT cell volume trajectories from **c** (solid lines), re-scaled in time and overlaid with *sqh*^{1} mutant data (dashed lines), demonstrating slower yet hierarchical cytoplasmic transport in the mutants.

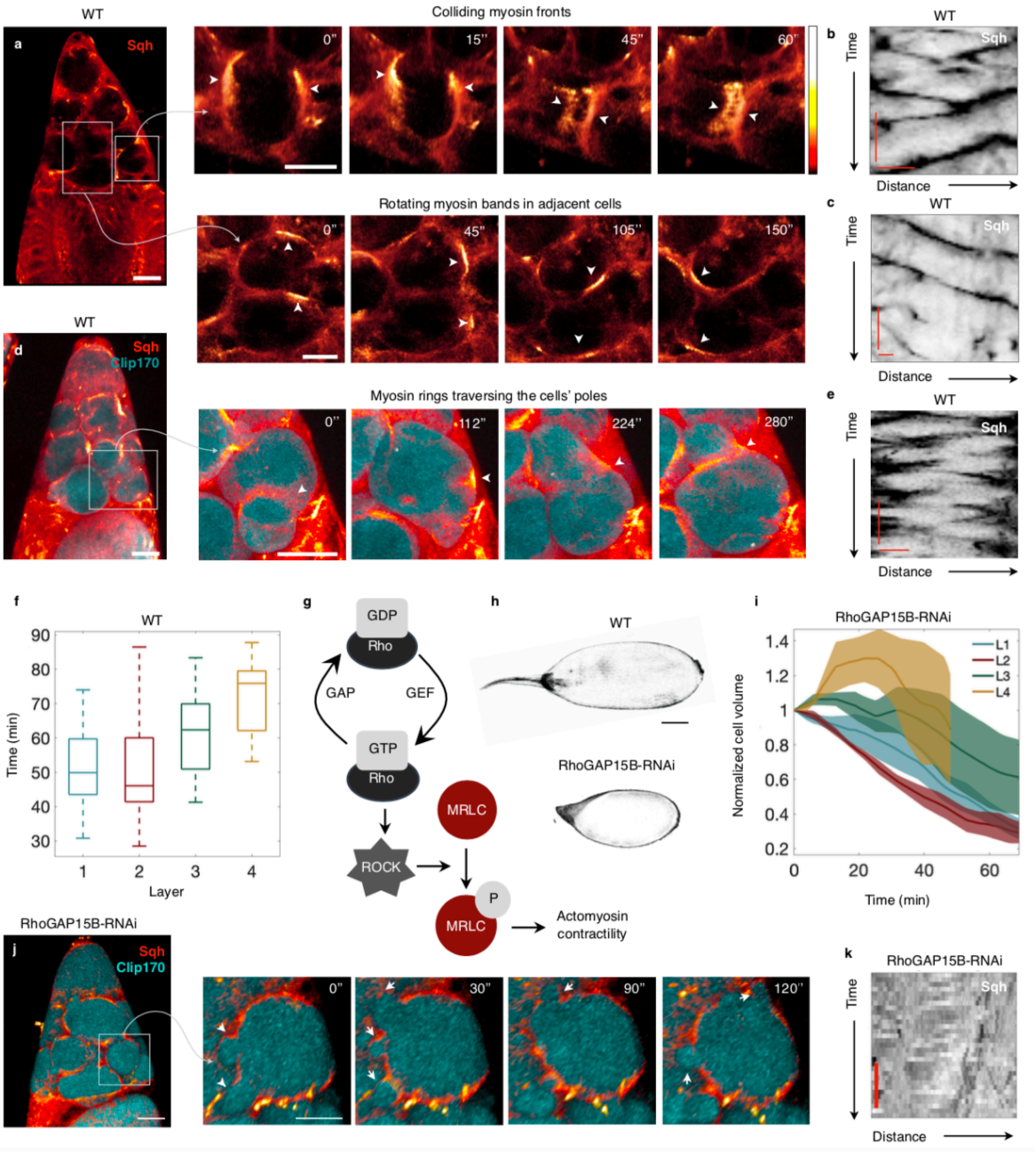

409

410 **Figure 3 | Phase II of NC dumping requires Rho-regulated wave-like actomyosin dynamics. a**, Heat

411 map of an egg chamber expressing *sqh-mCH*; blowups show NCs with dynamic actomyosin cortical

412 waves as colliding fronts (top) and rotating bands (bottom) in two adjacent cells, with respective

413 kymographs of Sqh intensity around NCs' perimeter (**b**, **c**). **d**, Heat map of an egg chamber expressing

414 *sqh::mCH* and *Clip170::GFP* (cyan); blowups show a NC with an actomyosin ring (arrowhead) traversing

415 the cell's opposing poles and deforming cell shape, with kymograph of Sqh intensity in **e**. **f**, Box-and-

whisker plot of median time at which nonuniform and persistent cell deformations are first observed following onset of NC dumping in each layer (center line = median; edges = upper and lower quartiles; whiskers extend to extrema; *N* = 20, 22, 16, 5 cells for layers 1, 2, 3, and 4). **g**, The Rho/ROCK signaling pathway regulates phosphorylation of the myosin regulatory light chain (MRLC) and actomyosin contractility. **h**, Comparison between wild-type (WT; top) and RhoGAP15B-depleted (bottom). Scale bar = 50 μm. **i**, Plot of normalized NC volumes during NC dumping for each layer from live imaging of RhoGAP15B knockdowns; *t* = 0 is onset of NC dumping; solid line indicates average; envelopes show standard error (*N* = 7, 6, 3, 2 cells for layers 1, 2, 3, and 4, respectively). The trajectory for Layer 4 stops at *t* ~ 50 minutes due to membrane breakdown. **j**, RhoGAP15B-depleted germline expressing *sqh::mCH* and *Clip170::GFP;* blowup shows smaller short-lived cell protrusions as opposed to cell-scale deformations observed in WT. **i**, Kymograph of Sqh intensity along the perimeter of a cell in a RhoGAP15B knockdown at a comparable time to **b**, **c**, and **e**, illustrating disrupted wave dynamics; black indicates highest intensity. Scale bar in **a**, **d**, and **j** = 40 μm; scale bar in blowups = 20 μm; kymograph scale bars in **b**, **c**, **e**, and **k** = 5 min; 10 μm.

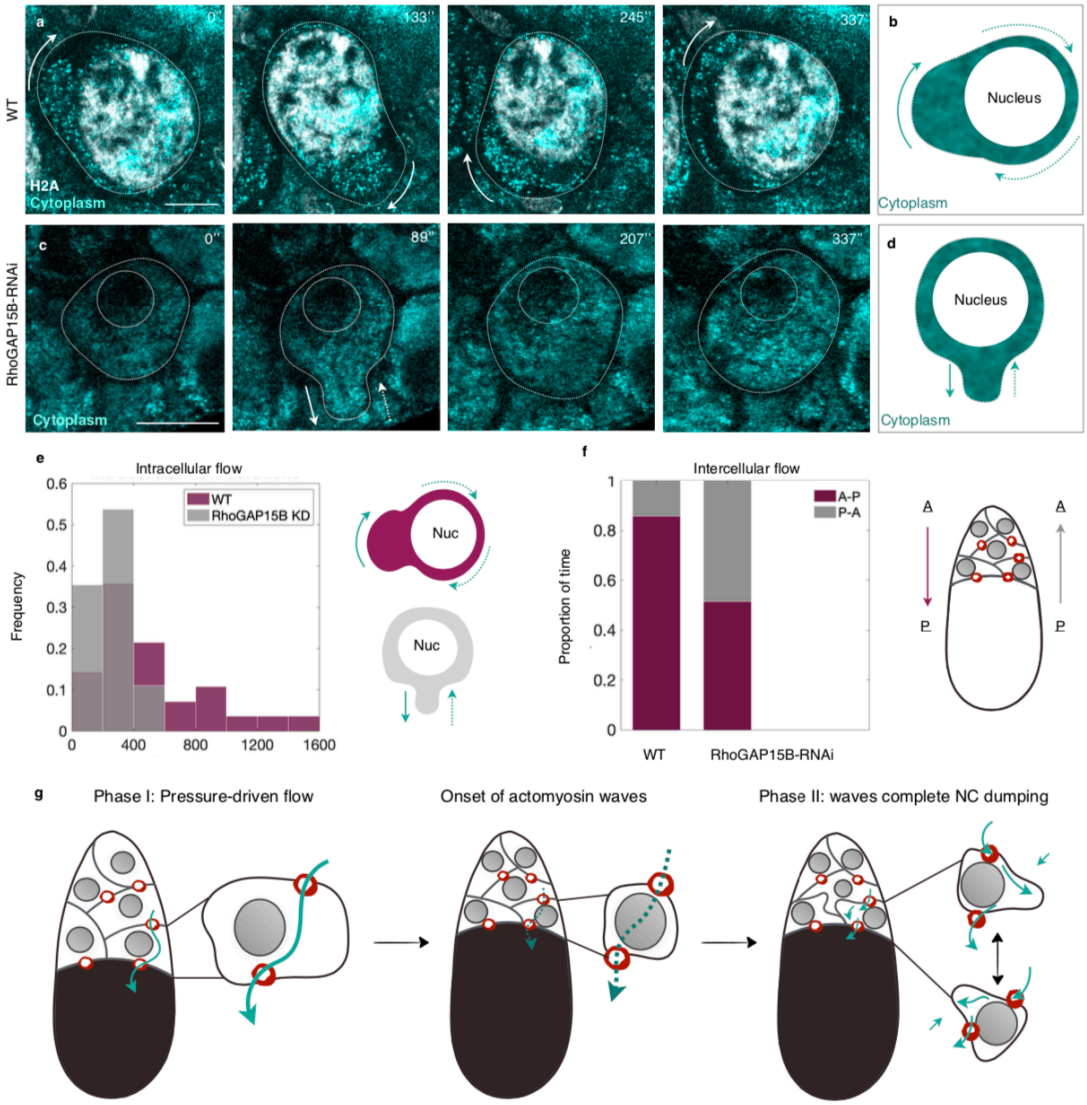

Figure 4 | Physical and biochemical mechanisms conspire to complete NC dumping. a, Time-lapse images from reflection-mode microscopy showing cytoplasm (cyan) flowing around a NC nucleus (H2A, white) as persistent actomyosin waves deform cell shape. **b**, Illustration of cytoplasmic flow observed in **a**, where arrows point in the direction of cytoplasmic flow. **c**, Erratic and short-lived cytoplasmic flow in a germline RhoGAP15B knockdown, illustrated in **d**, highlighting the lack of revolutionary motions observed in WT. Scale bars in **a** and **c** = 20 μm. **e**, Histogram of the duration of observed intracellular cytoplasmic flow events in WT and RhoGAP15B knockdowns (WT: *N* = 28 events; RhoGAP15B-RNAi: *N* = 82). **f**, Bar plot of proportion of time anterior-to-posterior (A-P) versus posterior-to-anterior (P-A) flows were observed in WT (30 minutes) and in RhoGAP15B-RNAi (54 minutes). **g,** Schematic of hypothesized model for the

454 contribution of surface tension-driven and actomyosin-dependent flows to directional and complete NC
455 dumping. Arrows show direction of intercellular flow; dashed arrow indicates interrupted flow; arrowheads
456 point to actomyosin-mediated cell deformations that permit continued intercellular flow in shrunken NCs.